SAND2018-6578J

AUTHOR QUERY FORM

AIP Publishing	**Journal: J. Appl. Phys.** **Article Number: 017824JAP**	**Please provide your responses and any corrections by annotating this PDF and uploading it according to the instructions provided in the proof notification email.**

Dear Author,

Below are the queries associated with your article; please answer all of these queries before sending the proof back to AIP.

Article checklist: In order to ensure greater accuracy, please check the following and make all necessary corrections before returning your proof.

1. Is the title of your article accurate and spelled correctly?
2. Please check affiliations including spelling, completeness, and correct linking to authors.
3. Did you remember to include acknowledgment of funding, if required, and is it accurate?

Location in article	Query / Remark: click on the Q link to navigate to the appropriate spot in the proof. There, insert your comments as a PDF annotation.
AQ1	Please check that the author names are in the proper order and spelled correctly. Also, please ensure that each author's given and surnames have been correctly identified (given names are highlighted in red and surnames appear in blue).
AQ2	Please provide report number for first part of Ref. 47; please provide page number for second part and also check the edits made in Ref. 47.

Thank you for your assistance.

J_ID: JAPIAU DOI: 10.1063/1.5026507 Date: 15-June-18 Stage: Page: 1 Total Pages: 9

JOURNAL OF APPLIED PHYSICS **123**, 000000 (2018)

Heating rate dependent ignition of Al/Pt nanolaminates through pulsed laser irradiation

AQ1 Michael J. Abere, Cole D. Yarrington, and David P. Adams
Sandia National Laboratories, Albuquerque, New Mexico 87123, USA

(Received 20 February 2018; accepted 5 June 2018; published online xx xx xxxx)

Direct laser irradiation of sputter deposited Al/Pt nanolaminate multilayers results in rapid local heating and exothermic mixing of reactant layers. Milli- and microsecond pulsed laser irradiation under certain test conditions leads to single-point ignition of rapid, self-propagating, formation reactions. Multilayers having bilayer thicknesses of 328 nm, 164 nm, and 65 nm are characterized by their ignition onset times and temperatures. Smaller bilayer thickness multilayers require less laser intensity for ignition compared with larger bilayer designs (when utilizing a particular pulse duration). The relationship between laser intensity and ignition onset time is used to calibrate an activation energy for ignition within a finite element reactive heat transport model. The local heating rate is varied from 10^4 K/s to 10^6 K/s by selecting a laser intensity. Kissinger analysis was performed on the heating rate-dependent ignition temperatures measured with high speed pyrometry to experimentally determine an activation energy in the foils of ($6.2 \pm 1.6 \times 10^4$ J/mole atoms). This value is then compared to an activation energy produced from model fits to an ignition onset time of 7.2×10^4 J/mole atoms. *Published by AIP Publishing.* https://doi.org/10.1063/1.5026507

I. INTRODUCTION

Reactive nanolaminates consist of alternating layers of metals, alloys, or compounds that undergo self-propagating high-temperature synthesis reactions when ignited.[1–4] The bimetallic systems are often fabricated using vapor deposition processes, such as electron beam evaporation or magnetron sputtering, and can be ignited through thermal,[5,6] mechanical,[5,7] or electrical[5] means. In addition to their applications in joining,[8,9] brazing,[10] sealing,[11] and ignition of secondary reactions,[12] these materials offer an ideal uniform system to study reactions and phase transformations subjected to rapid heating and large compositional gradients.[13–16] The heating rate in the self-propagating front can be as fast as 10^7 K/s in Ni/Al[14] and over an order of magnitude greater in the more energetic Al/Pt bimetallic system.[17] Reactions under these conditions have been shown to form unique product phases.[18] Intermediate heating rates between 10^4 K/s and 10^5 K/s have also been shown to change the phase formation sequence in a few nanolaminate systems[19,20] compared with that developed at heating rates of 10° to 10^2 K/s utilized in traditional calorimetry.

To characterize the kinetic properties that underly mixing and reaction, experimental data are typically used to parameterize numerical models through a combination of analytical expressions,[21–27] continuum[13,28–33] and molecular dynamics[13,34–37] simulations. These models describe ignition and steady wave propagation as a function of design parameters such as the bilayer thickness[24,38] and premixed volumes.[23,24] Recent work has shown the importance of experimental verification across a range of temperatures and heating rates as the data near the lower heating rates for ignition are not represented well with models calibrated to steady state wave measurements.[5,13,19] By calibrating across a range of heating conditions, the full range of temperature dependence on mass transport can be determined to alleviate this discrepancy.[13]

This work uses pulsed laser irradiation to investigate reactive nanolaminate ignition at different heating rates spanning the range from 10^4 K/s to 10^6 K/s, with the larger rate being an order of magnitude faster than high heating rate calorimetery[19,20] and the lower rate approximately two orders above hot plate ignition.[5] Our study focuses on equiatomic Al/Pt, a system chosen for its high exothermicity,[39] consistent propagation behavior,[18] and low predicted pulsed laser ignition temperatures easily measurable with commercial pyrometers.[17] Unlike most heating methods, laser ignition also allows for the direct characterization of the local ignition zone. Specifically, there is direct optical access during laser heating which makes locally focused pyrometry and high-speed videography possible. Quantitative analysis of the nanolaminate's laser-materials response through both Kissinger analysis and a finite element reactive heat transport model is then used to calculate and interpret the activation energy of ignition.

II. METHODS

The reactive multilayers for this work were deposited with direct current magnetron sputtering on a Unifilm Company system having a base pressure of 5×10^{-7} Torr.[18] The alternating layers of Al and Pt were deposited onto oxidized Si substrates with a one-to-one stoichiometry starting with a Pt layer. The total film thickness was held constant at ~1640 nm, and the bilayer thickness was varied to 65 nm, 164 nm, and 328 nm. Cross sectional scanning transmission electron microscopy confirmed that the variation in the layer thickness was <3 nm with an amorphous premixed interlayer at each interface that varied between 8 nm and 11 nm,

J_ID: JAPIAU DOI: 10.1063/1.5026507 Date: 15-June-18 Stage: Page: 2 Total Pages: 9

consistent with the average premixed thickness reported in previous work.[18]

The ignition experiments were performed via laser heating of the Pt surface of free-standing foils. To be clear, the deposited films were separated from their Si substrates and all experiments irradiated the first deposited Pt layer. This was done because Pt is the smoother of the two surfaces and thus minimizes contributions from field enhancement during laser absorption that could arise at a surface asperity. The heat source for laser ignition was a Northrop-Grumman eDriveTM 20 W diode laser with a central wavelength of 808 nm. The laser pulse duration was set between 10 000 μs and 500 μs as measured using a fast photodiode. The rise time of each pulse was much less than the laser pulse durations. The laser was focused using a Mitutoyo 5× microscope objective to a flat-top beam profile with <10% ripple within the full width half maximum as described in Ref. 40. Under these focusing conditions, a beam radius, ω_0, of 155 ± 5 μm was measured using a WinCamD beam profiling camera. Laser intensity is nominally reported as the on-surface value after accounting for losses in the optical delivery system, and absorbed intensity can be calculated by multiplying this value by one minus the Pt reflectivity. The small total thickness and large thermal conductivity of the material (estimated to be on the order of 10^2 W/m·K[41]) allow for the assumption that the laser uniformly heats a foil in the transverse direction at lower heating rates on the order of 10^4 K/s.[17] The irradiation conditions for which this assumption breaks down and the laser must be treated explicitly as a surface heating technique will be discussed below. Videography recorded the foil over the timespan between the leading edge of the pulse and the reacted foil breaking apart, using a Phantom v12 high-speed camera with an interframe time of 1.79 μs. Timing for the leading edge of each pulse was determined by subtracting the measured duration from the last high speed camera frame with transmitted laser light and setting the camera acquisition window accordingly. This experimental setup allows for temporal resolution of ignition onset equal to the interframe time, which is at least two orders of magnitude shorter than the laser heating time for all pulse durations tested. Temperature measurements prior to ignition were performed within the laser heated zone using a Metis H318 pyrometer aligned to the laser beam location on the back (Al) side of the foil using a fiducial mark placed on the screen of an *in-situ* microscope and camera. The pyrometer has an interframe time of 200 μs, a spot diameter of 300 μm, and emissivity calibrated to thermocouple measurements of a ~1.6 μm thick Al foil on a hot plate. The reaction onset time is considered to be the frame of first light emission in the high-speed videography based on the method described in Ref. 40. The timestep at which the pyrometer jumps from under 700 °K to over 1000 °K (the detector's upper bound) is less than 20 μs. This observed temperature behavior is indicative of a transition from a laser heating regime to a propagating flame within the model described below.

A finite element reactive heat transport model was developed and used to investigate ignition and its underlying processes. This model was implemented in Aria, a Galerkin finite element based heat transfer code developed and maintained by Sandia National Laboratories, and module in the SIERRA computational framework.[42] The nanolaminate is treated as a continuum in a 2D axisymmetric finite element model and uses a diffusion limited sub-grid model to track conversion from reactants (Al/Pt) to products (Al_xPt_y) in the form of product layer thickness. The reactive multilayer is shown schematically in Fig. 1. Here, Δ is the bilayer thickness, which is subdivided into segments of a_0 and b_0 equal to half of the nominal thickness of the Pt and Al layers with no intermixed layer for a given bilayer design, respectively. For the initial conditions at time t = 0 on the left side of Fig. 1, s(0) is set to 10 nm for each bilayer design to account for the premixed interfacial layer formed during deposition.[18] As the foil reacts (left to right in Fig. 1), the product layer thickness, s(t), increases while depleting the reactant half-layers to thicknesses of a(t) and b(t). This conversion proceeds per the governing rate described in the following equation:

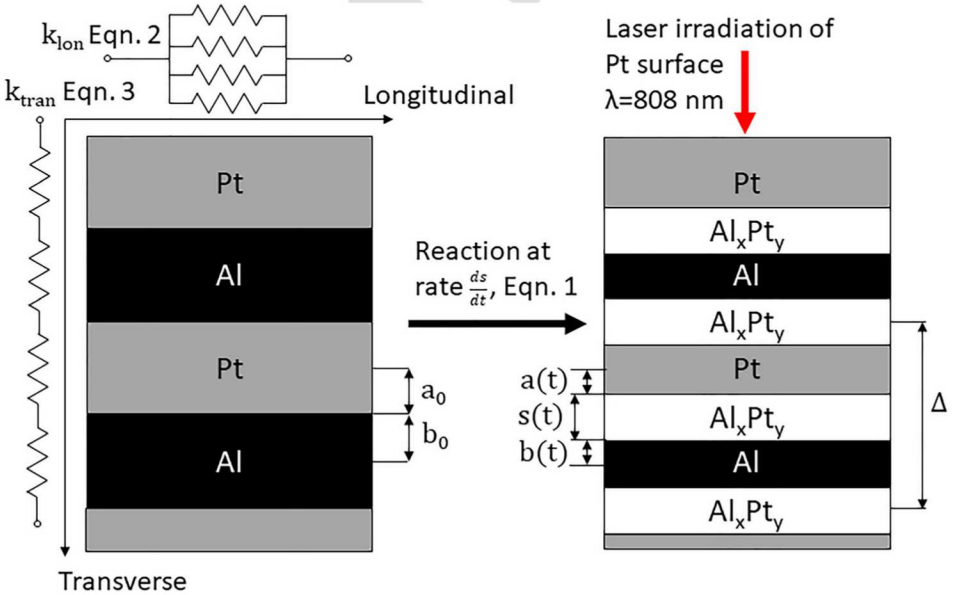

FIG. 1. This diagram shows the Al/Pt multilayer notation with bilayer thickness Δ for the reaction model and depicts the progression from pristine Al/Pt to the growth of a product layer of thickness s(t) with composition Al_xPt_y upon laser irradiation. Here, a(t) and b(t) are the half thicknesses of the Pt and Al layers at time t, respectively. A thermal circuit model for calculating the foil thermal conductivity, k, in the longitudinal and transverse directions is shown schematically on the left. Individual material layer widths are not drawn to scale. Within the simulation, s(0) = 10 nm to account for the premixing in the as deposited nanolaminate.

J_ID: JAPIAU DOI: 10.1063/1.5026507 Date: 15-June-18 Stage: Page: 3 Total Pages: 9

$$\frac{ds}{dt} = \frac{D_0 \exp\left(\frac{-E_A}{RT}\right)\left(1+\frac{a_0}{b_0}\right)}{s(t)}, \quad (1)$$

where E_A is an effective activation energy of the global reaction, R is the gas constant, D_0 is a diffusion coefficient, and T is the temperature. The growth rate of the product layer thickness is described by the reaction model derived in Ref. 43. In the continuum model, the layered structure is assumed to have a square wave concentration profile in the transverse direction. As the simulation steps forward in time, the product layer thickness increases depending on both the growth rate defined by Eq. (1) and the energy from reaction. The rate equation can be classified as diffusion limited, meaning that it is based on an Arrhenius diffusion relationship that decreases with increasing product layer thickness [i.e., s(t), the product layer thickness, is in the denominator of Eq. (1)]. The rate law described in Eq. (1) is coupled to the governing equations through the heat generated at each time step. The increase in the AlPt thickness is proportional to the heat generated in the reaction, and this heat is added as a volumetric heating term in the energy conservation equations. To take into account the added stiffness due to volumetric heating, the reaction species equations are subcycled adaptively. Further details of the model can be found in Ref. 17.

Laser heating is modelled as a radially varying Gaussian flux boundary condition with magnitude equal to the incident intensity reported from experiment minus the Pt reflectivity on the top surface extending from the axis of symmetry to a distance equal to the beam radius of ω_0. Two different models of nanolaminate thermal conductivity, k, are compared (1) an isotropic rule of mixtures and (2) a thermal circuit model from Ref. 28 with resistors in parallel and in series in the longitudinal and transverse directions of the foil, respectively, as shown schematically in Fig. 1. The longitudinal thermal conductivity, $k_{lon}(t,T)$, and transverse thermal conductivity, $k_{tran}(t,T)$, are calculated from Eqs. (2) and (3), respectively,

$$k_{lon}(t,T) = \frac{k_{Al}(T)F(t)}{w(t)} + \frac{k_{Pt}(T)F(t)(w(t)-1)}{w(t)} + k_{AlPt}(T)[1-F(t)], \quad (2)$$

$$k_{tran}(t,T) = \left(\frac{F(t)}{k_{Al}(T)w(t)} + \frac{F(t)(w(t)-1)}{k_{Pt}(T)w(t)} + \frac{1-F(t)}{k_{AlPt}(T)}\right)^{-1}, \quad (3)$$

where a progress variable F(t) is defined as $1-s(t)/(b_0 \cdot w(t))$ and w(t) is $1+a(t)/b(t)$. Within the 2D axisymmetric model, the thermal conductivity at tensor (i,j) is given in Eq. (4). The 2D axisymmetric assumption was justified by the very small Biot number, indicating that heat transfer within the material in the transverse direction occurs on a much faster time scale than bulk heating. A mesh size of 400 nm was employed, resulting in a mesh depth of 4 in the transverse direction. Values for the material property input into the model are summarized in Tables I and II in the Appendix

$$k_{ij}(t,T) = \begin{bmatrix} k_{lon}(t,T) & 0 & 0 \\ 0 & k_{lon}(t,T) & 0 \\ 0 & 0 & k_{tran}(t,T) \end{bmatrix}. \quad (4)$$

III. RESULTS AND DISCUSSION

Ignition of the Al/Pt nanolaminate foils in response to laser irradiation is defined as the rapid local mixing and reaction of metal species within a multilayer that gives rise to a self-propagating, higher temperature, formation reaction that continues to the freestanding edges of a mounted specimen. Ignition originates at the center of the irradiated zone, and the reaction wave reaches a near constant velocity within tens of microns beyond the laser spot radius. Outside the irradiated zone, the reaction was observed to self-propagate at a steady measured front velocity of 14 m/s, 34 m/s, and 64 m/s in the 328 nm, 164 nm, and 65 nm bilayer designs, respectively.

An ignition onset time is measured as the time between the leading edge of the pulse and first light emission by the reactive material as viewed in a high speed videograph. Figure 2(a) shows the relationship between laser intensity and ignition onset time for four descriptive experiments in a 164 nm bilayer foil. In the case shown in Fig. 2(b), a 1000 μs pulse at 930 W/cm^2 does not ignite the foil, which corresponds to an infinite ignition onset time in Fig. 2(a). Increasing the pulse duration to 5000 μs at the same laser intensity leads to ignition 2260 μs into the pulse as shown in Fig. 2(c). In order to ignite the foil with the 1000 μs pulse, the laser intensity must be increased to 1440 W/cm^2 as shown in Fig. 2(d). The minimum intensity for a given pulse duration capable of igniting the foil is referred to in this document as the go/no go threshold intensity. This condition occurs when the ignition onset time is equivalent to the pulse duration. Increasing the laser intensity above the go/no go threshold value to 1880 W/cm^2 leads to ignition during the pulse after 640 μs for the 1000 μs pulse as shown in Fig. 2(e).

The different cases of the material response to laser irradiation listed in Fig. 2 are plotted for five pulse durations in each of three different bilayer designs in Fig. 3. The ignition onset time decreases with increasing laser intensity for each of the nanolaminate designs shown in Fig. 3. The ignition onset time for a given laser intensity is independent of the pulse duration, which leads to a single continuous relationship in each plot. Furthermore, the relationship between ignition onset time and go/no go threshold for the 1000 μs pulses in Fig. 2 is consistent across all pulse durations and bilayer thicknesses tested. This can be seen graphically in Fig. 3 where the intensity at which an experimental data point intersects the dotted guideline of its pulse duration corresponds to the measured go/no go threshold. To restate, the physical significance of the threshold laser intensity is the point at which the dwell time required to ignite the foil for local heating with a given photon density is equal to the pulse duration for ms and μs long laser pulses.

The relationships between laser ignition thresholds for different pulse durations and bilayer designs are also apparent in Fig. 3. For each bilayer, the mean value for laser ignition threshold intensities for 10 000 μs, 7500 μs, and 5000 μs

J_ID: JAPIAU DOI: 10.1063/1.5026507 Date: 15-June-18 Stage: Page: 4 Total Pages: 9

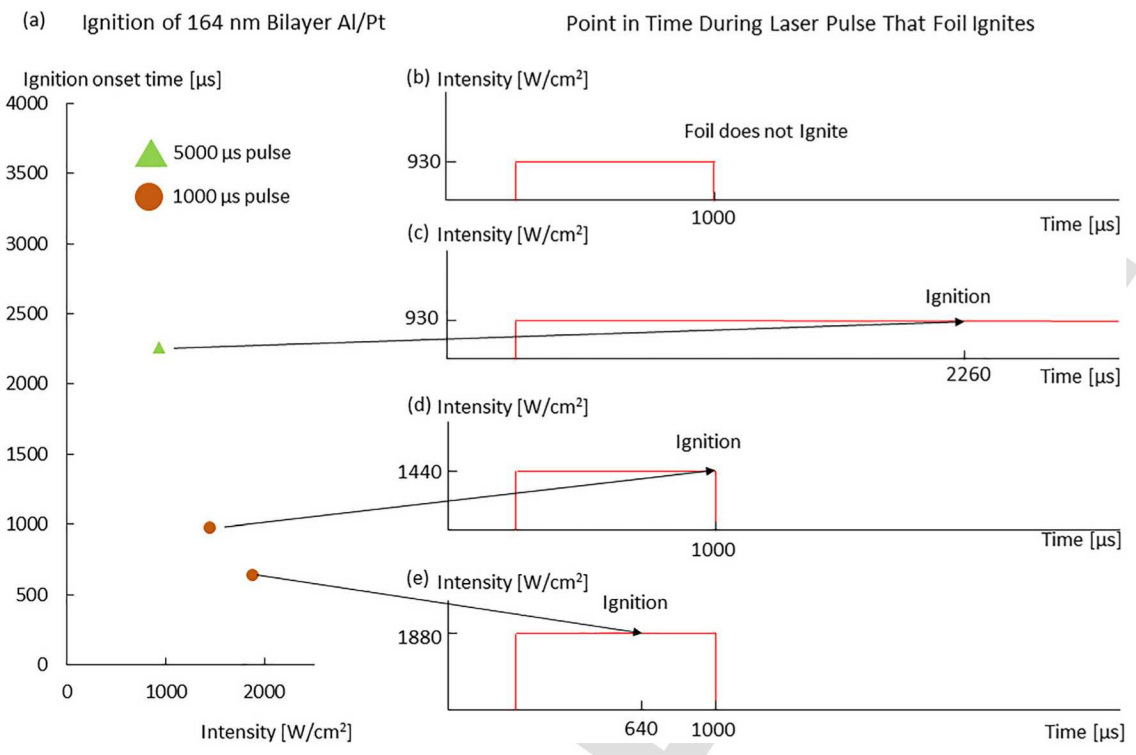

FIG. 2. The graph in (a) shows the relationship between laser intensity and ignition onset time for four experiments in (b)–(e) for a 164 nm bilayer Al/Pt foil. For each of the laser pulses plotted in [(b)–(e)], note that the rise time ≪ pulse duration and thus appears as a delta function. In (b), the 1000 μs pulse at 930 W/cm^2 does not ignite the foil. Increasing the pulse duration to 5000 μs at the same intensity in (c) leads to ignition after 2260 μs. In order to ignite the foil at the end of a 1000 μs pulse, the intensity must be increased to 1440 W/cm^2 in (d). This intensity corresponds to the go/no go threshold for the 1000 μs pulse. Further increasing the intensity of the 1000 μs pulse to 1880 W/cm^2 leads to ignition during the pulse after 640 μs.

pulses increases with decreasing pulse duration but is separated by less than the error arising from experimental variability. However, the go/no-go thresholds for the 1000 and 500 μs experiments are clearly separated thereby demonstrating a pulse duration dependence on the ignition threshold. The threshold intensity for 500 μs pulses is a factor of ~1.5 less than that for 1000 μs for all three bilayer designs.

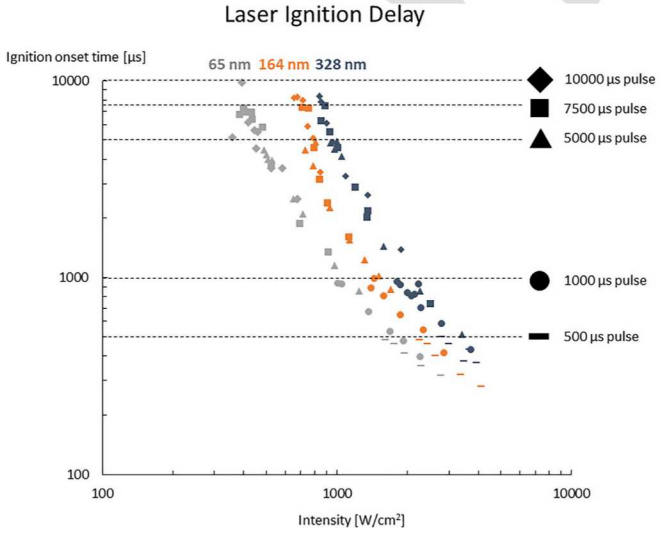

FIG. 3. This graph depicts the relationship between laser intensity and ignition onset time for Al/Pt bilayer thicknesses of 65 nm, 164 nm, and 328 nm. For each bilayer design, the go/no go threshold for a specific laser pulse duration corresponds to the laser intensity at which the ignition onset time equals the pulse duration.

Decreasing the bilayer thickness between 328 nm and 65 nm reduces the laser ignition threshold at each pulse duration. This trend agrees with previously reported laser ignition thresholds both specifically in Al/Pt[4] and more generally in reactive nanolaminates.[6] The range of Δ chosen for this work lies in the regime of bilayer thicknesses where propagation velocity is inversely correlated with the power density necessary for ignition. In this regime, the foil sensitivity increases with decreasing Δ due to the increased interfacial density and corresponding reduction in diffusion path length necessary for atomic mixing. It should, however, be noted that reducing bilayer thickness to a length at which a decrease in the steady-state propagation velocity is observed due to contributions from a larger volume fraction of premixed material with lower chemical potential energy would result in an increase in the laser ignition threshold.[4]

For a given bilayer design, increasing laser intensity also raises the ignition temperature as shown in the pyrometry data of the 164 nm bilayer in Fig. 4. The increase in laser intensity corresponds to a faster heating rate that in general results in the higher observed ignition temperature.[44,45] In the pyrometry measurements shown in Fig. 4, a heating rate of 2.3×10^4 K/s corresponds to an incident laser intensity of 657 W/cm^2, while a heating rate on the order of 10^5 K/s corresponds to the laser's maximum output of ~1000 W/cm^2 for the 155 μm focused beam radius. Although the pyrometer was unable to collect enough light at the short acquisition times necessary to measure ignition temperatures at the highest (~4000 W/cm^2) laser intensities tested, the finite element simulations predict that those heating rates are on the order of 10^6 K/s.

ID: aipepub3b2server Time: 16:48 I Path: D:/AIP/Support/XML_Signal_Tmp/AI-JAP#181008

J_ID: JAPIAU DOI: 10.1063/1.5026507 Date: 15-June-18 Stage: Page: 5 Total Pages: 9

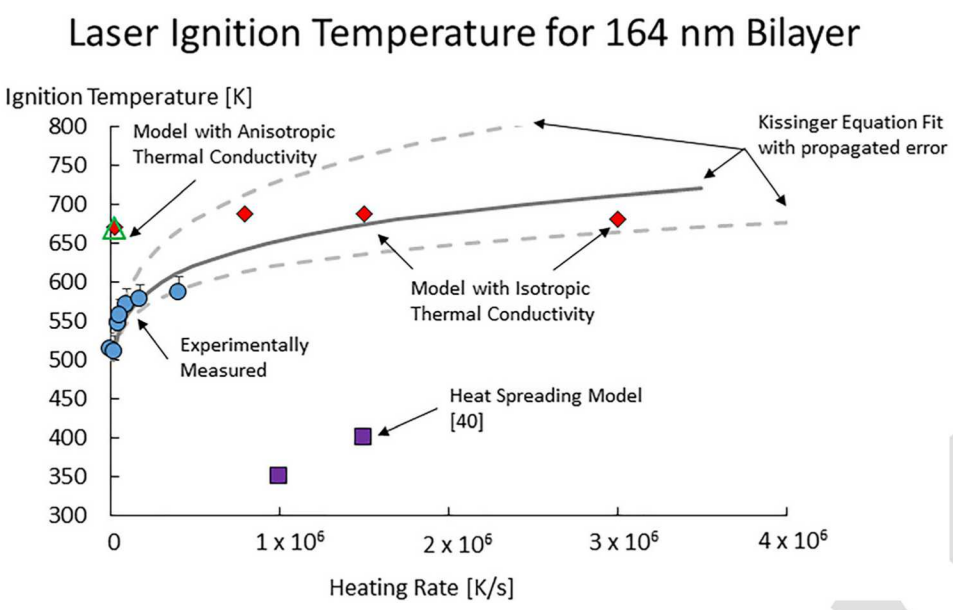

FIG. 4. This graph shows the relationship between heating rate and ignition temperature in the 164 nm Al/Pt foil. The experimentally measured temperatures from high speed pyrometry are fit to the Kissinger-Akahira-Sunose Equation with an error band determined by propagation of the instrumental uncertainty in the pyrometer. These values are compared to model values from this work and Ref. 40.

From this physical understanding of the pulsed laser ignition threshold of reactive nanolaminates, it is now possible to predict the ignition onset time for a given laser intensity using a diffusion-limited single step reaction mechanism within a finite element reactive heat transport simulation. This is performed by calculating the time at which the reactants are completely transformed to product at the spot center. In previous work, an E_A of 7.2×10^4 J/mole atoms for these calculations was determined by fitting it in the model to match the ignition delay time for a single laser intensity of 790 W/cm^2 in a 164 nm bilayer foil.[17] While most material properties used in the model were obtained from the literature, the thermal conductivity of the product phase was also calibrated from the same experimentally measured ignition delay time. This resulted in a product phase thermal conductivity of 70 W/m·K. In this work, the pyrometry measurements of laser heating rate dependent ignition temperatures were used to validate model predictions of E_A. A value of $6.2 \pm 1.6 \times 10^4$ J/mole atoms is calculated by performing isoconversional analysis with the Kissinger-Akahira-Sunose[46,47] equation on the measured ignition temperatures at different laser heatJ/ing rates shown in Fig. 4. The reported error band included in the figure (indicated with dashed lines) represents a propagation of the instrumental uncertainty in the pyrometer. The Kissinger-Akahira-Sunose equation is provided in Eq. (5) below with β defined as the heating rate. T_{ig} represents ignition temperature. The reported error in this calculation represents the uncertainty as to when, within the pyrometer's time step, ignition occurs between the last measured point before the heating rate increases by more than two orders of magnitude as the foil ignites. The previously fit value to ignition onset time in the 164 nm bilayer is considered valid for the simulations in this work as it falls within this range

$$ln\left(\frac{\beta}{T_{ignition}^2}\right) = Constant - \frac{E_A}{RT_{ignition}}. \quad (5)$$

The calculated relationship between laser intensity and ignition onset time is shown in comparison to the measured values using Fig. 5. For the 164 nm bilayer design in Fig. 5, the simulations accurately fit the experimental data independent of the thermal conductivity model used. Calculating thermal conductivity with either an isotropic rule of mixtures or an anisotropic thermal circuit model produced a linear correlation factor of 0.99 and 0.98 to the experimental data, respectively. This model fitting over all tested laser pulse durations corresponds to three orders of magnitude in foil heating rate.[17] Differences were found when investigating the thinner bilayer design. In this case, the anisotropic model showed an improved fit for the thinner 65 nm bilayer design. Figure 5 shows an increase in the linear correlation factor

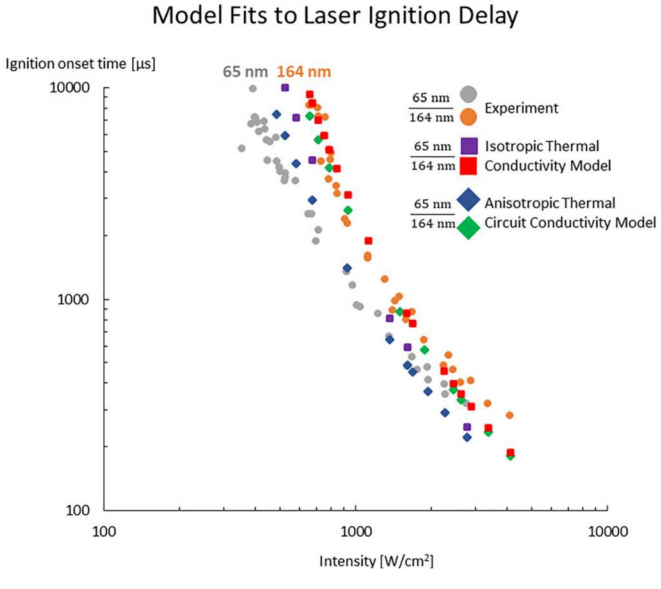

FIG. 5. The model fits to ignition onset time comparing an isotropic thermal conductivity model to an anisotropic thermal circuit model for the 164 nm and 65 nm bilayer designs of Al/Pt. While both models have linear correlation factors ≥0.98 for the 164 nm bilayer data, the use of the anisotropic thermal model for the 65 nm bilayer improves linear correlation from 0.65 to 0.81.

between the model and experiment from 0.65 to 0.81 by implementing the thermal circuit model. Due to the decades of difference in ignition onset time tested, the calculated correlation factors should be considered as predominately a measure of model fit for the millisecond laser pulses.

The reduced linear correlation between the model and experiment when decreasing bilayer thickness from 164 nm to 65 nm likely arises because the thermal circuit model does not explicitly account for all of the thermal transport physics within the nanolaminates. The thermal circuit model does not have a term for interface scattering as a mixed (metallic and covalent/ionic) bonded intermetallic interface grows into the metallically bonded reactants.[48] The number of these thermal scattering sites increases from 40 to 100 between the 164 nm and 65 nm bilayer foils. Moreover, the amorphous premix phase has a reduced thermal transport due to a lower density of states for heat transport within the electron system.[49] The volume fraction of the disordered phase increases from 12% in the 164 nm bilayer nanolaminate to 30% volume fraction in the thinner design.

Predicted ignition temperatures for different heating rates based on Eq. (5) are plotted in Fig. 4 for activation energy across the range of $6.2 \pm 1.6 \times 10^4$ J/mole atoms with a solid curve for the median E_A value bookended by dashed curves to show the range of potential ignition temperatures based on the propagated error in the calculation of E_A. For heating rates on the order of 10^6 K/s from irradiation on the order of 4000 W/cm^2, the calculated ignition temperatures at the higher rates fall within the error propagated range from Kissinger analysis. This contrasts with the much lower ignition temperatures shown in Fig. 4 that are predicted from a pure heat spreading model[40] demonstrating the importance of incorporating the reactive heat equation into the continuum model. However, the reactive model in this work breaks down when predicting ignition temperature at lower heating rates of $\sim 10^4$ K/s from irradiation at 660 W/cm^2 regardless of whether an isotropic or thermal circuit model is used for the 164 nm bilayer, which suggests that the disparity does not originate from model inputs for ground state thermal conductivity. Moreover, the ignition temperatures from the continuum model do not follow the shape of an isoconversional relationship and begin to decrease with higher heating rate at 3×10^6 K/s.

There are several potential sources for the disparity between the experiment and simulation that arise because the current model is not accounting for dynamic thermal properties arising from material phase evolution during ignition. Compared to the 10^6 K/s heating rates, one fundamental difference during ignition at 10^4 K/s is that radial heat loss occurs faster than the laser can heat the ignition zone.[17] This in turn leads to pre-ignition reactions and the observed temperature deficit in the high-speed videography in Ref. 17. In this lower regime of heating rates, the global single step reaction mechanism is not accounting for the heat of reaction from the evolution through intermediate phases. The resulting overestimate of ignition temperature in Fig. 4 indicates that the pre-ignition phase formation likely involves less exothermic reactions. With regard to model predictions at higher heating rates, the decrease in the predicted ignition temperature at 3×10^6 K/s with respect to slightly larger values at a reduced heating rate of 8×10^5 K/s corresponds to laser irradiation conditions at which the go/no go threshold intensity has greatly increased over lower heating rates as shown in Fig. 3. This higher threshold intensity is indicative of the inclusion of an additional conductive pathway for heat loss in the foil's transverse direction as the laser must be considered as a surface heating source for heating on shorter timescales. Under these conditions, the uniform heating assumption based on the time independent Biot number has likely broken down. Thus, the laser heating rates on the order of 10^6 K/s represent the boundary for the applicability of the existing mesh within the finite element model for the 1.6 μm- thick foil. This boundary condition to the model assumptions can be further seen in Fig. 5 where an increasing percentage error becomes apparent on the log-log plot at the highest laser intensities.

In comparing the finite element model to laser induced reaction of this bimetallic system, the balance between thermal and mass transport in determining reaction kinetics becomes clear. In contrast to the thermal transport properties, the correspondence between Kissinger analysis of pyrometry data and the continuum model fit to ignition onset time in determining an effective activation energy of reaction shows that a single-step reaction diffusion limited mechanism is adequately capturing the underlying mass transport properties of ignition. Additionally, the insensitivity of the effective activation energy of ignition to the dynamic nature of thermal transport indicates that this term is dominated by the portion of the activation energy attributable to mass diffusion. Both the Kissinger analysis and continuum model values are consistent with a previously reported activation energy for mass diffusion of Al into a metastable amorphous Al-Pt phase of 6.9×10^4 J/mole atoms,[50] a likely pathway for the solid-state mixing during ignition. Furthermore, the three orders of magnitude in heating rate covered within this study demonstrate the viability of laser irradiation experiments to explore reaction kinetics at a tunable heating rate and motivates the use of shorter nanosecond laser pulses to match heating rates to those within the propagating wave. This will allow for a bridging of the disparate kinetics between ignition and propagation in reactive multilayers that are typically treated as parallel systems.

IV. SUMMARY

Laser irradiation experiments were performed on equiatomic Al/Pt nanolaminates with bilayer thicknesses of 328 nm, 164 nm, and 65 nm. High speed videography showed that the laser ignition onset time is a continuous function of laser intensity, and pyrometry showed that higher heating rates associated with larger laser intensities result in increased ignition temperature. A finite element reactive heat transport model was fit to the experimental data, showing that the kinetic pathway to ignition is governed by an activation energy attributable to mass transport and can be captured as a single step diffusion limited mechanism. While a thermal circuit model improves upon a simple rule of mixtures description of thermal transport, the reduced correlation between the model and experiment for smaller bilayer

J_ID: JAPIAU DOI: 10.1063/1.5026507 Date: 15-June-18 Stage: Page: 7 Total Pages: 9

thicknesses shows the need for an expanded understanding of transport across the initial amorphous premixed layers to more accurately model bilayers with substantial premixed volume before then considering the dynamic thermal properties of the reacting foil during the ignition event.

ACKNOWLEDGMENTS

The authors would like to thank Cathy Sobzak for operation and maintenance of vacuum deposition system. Sandia National Laboratories is a multimission laboratory managed and operated by National Technology and Engineering Solutions of Sandia, LLC, a wholly owned subsidiary of Honeywell International, Inc., for the U.S. Department of Energy's National Nuclear Security Administration under Contract No. DE-NA0003525. SAND NO. _2018-XXXXP.

APPENDIX: MODEL PARAMETERS AND MATERIAL PROPERTIES

Table I lists the nanolaminate design and model parameters. Constituent molecular weights, densities, Δ, and the 1:1 stoichiometry were used to define a_0 and b_0. a_i and b_i were determined similarly by defining $s_i = 10$ nm and subtracting from Δ.

The Al and Pt columns in Table II refer to properties of the pure elements. The third column titled AlPt refers to the mixture properties of the subgrid material model derived from the constituents, which is necessary to represent the nanolaminate as a continuum. AlPt does not represent the properties of the product phase.

TABLE I. Initial conditions and parameter values for the diffusion-limited product layer growth model. Subscript i is the initial condition used for the simulations and includes an initial product layer of 10 nm.

E_a,J/mole atoms	7.194
D_0, m^2/s	2.3×10^{-7}
s_i (nm)	10
a_0 (nm)	15.5;78;39
b_0 (nm)	17;86;43
a_i (nm)	10.7;73.2;34.2
b_i (nm)	11.8;80.8;37.8
$\Delta = 2(a_0 + b_0)$ (nm)	328;164;65

TABLE II. Material properties of aluminum, platinum, and AlPt.

Property	Description	Al	Pt	AlPt
H_f (J/kg)	Enthalpy of Formation	0	0	-0.904×10^6
M_w (kg/kg·mole)	Molecular weight	27	195	222
T_m (K)	Melting point	933.5	2041.4	933.5,2041.4
H_{fus} (J/kg)	Latent enthalpy	0.397×10^6	0.114×10^6	0.0483×10^6
C_{eff} (J/kg·K)	Effective C at T_m	79 400	22 800	9660;20 000
T_b (K)	Boiling point	2792.2	4098.2	Unknown
C (J/kg·K)	Specific heat	896.9	132.8	226
ρ (kg/m^3)	Density	2700	21 500	11 600
K (W/m·K)	Thermal conductivity	237	71.6	Eq. (4)

[1]E. Ma, C. V. Tompson, L. A. Clevenger, and K. N. Tu, Appl. Phys. Lett. **57**, 1262 (1990).
[2]A. S. Rogachev, Russ. Chem. Rev. **77**, 21 (2008).
[3]T. P. Weihs, "Fabrication and characterization of reactive multilayer films and foils," in *Metallic Films for Electronic, Optical and Magnetic Applications*, edited by K. Barmak and K. Coffey (Woodhead Publishing Limited, Philadelphia, PA, 2014), pp. 160–243.
[4]D. P. Adams, Thin Solid Films. **576**, 98 (2015).
[5]G. M. Fritz, S. J. Spey, Jr., M. D. Grapes, and T. P. Weihs, J. Appl. Phys. **113**, 014901 (2013).
[6]Y. N. Picard, J. P. McDonald, T. A. Friedmann, S. M. Yalisove, and D. P. Adams, Appl. Phys. Lett. **93**, 104104 (2008).
[7]S. C. Kelly and N. N. Thadhani, J. Appl. Phys. **119**, 095903 (2016).
[8]J. Wang, E. Besnoin, A. Duckham, S. J. Spey, M. E. Reiss, O. M. Knio, M. Powers, M. Whitener, and T. P. Weihs, Appl. Phys. Lett. **83**, 3987 (2003).
[9]A. J. Swiston, Jr., T. C. Hufnagel, and T. P. Weihs, Scr. Mater. **48**, 1575 (2003).
[10]D. P. Adams, M. M. Bai, M. A. Rodriguez, J. J. Moore, L. N. Brewer, and J. B. Kelley, in Proceedings of the 3rd International Brazing and Soldering Conference (Colorado, 2006).
[11]J. Braeuer, J. Besser, M. Wiemer, and T. Gessner, Sens. Actuators, A **188**, 212 (2012).
[12]J. P. McDonald, M. A. Rodriguez, E. D. Jones, and D. P. Adams, J. Mater. Res. **25**, 718 (2010).
[13]L. Alawieh, T. P. Weihs, and O. M. Knio, Combust. Flame **160**, 1857 (2013).
[14]J. C. Trenkle, L. J. Koerner, M. W. Tate, N. Walker, S. M. Gruner, T. P. Weihs, and T. C. Hufnagel, J. Appl. Phys. **107**, 113511 (2010).
[15]J. S. Kim, T. LaGrange, B. W. Reed, M. L. Taheri, M. R. Armstrong, W. E. King, N. D. Browning, and G. H. Campbell, Science **321**, 1472 (2008).
[16]A. S. Rogachev, S. G. Vadchenko, and A. S. Mukasyan, Appl. Phys. Lett. **101**, 063119 (2012).
[17]C. D. Yarrington, M. J. Abere, D. P. Adams, and M. L. Hobbs, J. Appl. Phys. **121**, 134301 (2017).
[18]D. P. Adams, M. A. Rodriguez, C. P. Tigges, and P. G. Kotula, J. Mater. Res. **21**, 3168 (2006).
[19]P. Swaminathan, M. D. Grapes, K. Woll, S. C. Barron, D. A. LaVan, and T. P. Weihs, J. Appl. Phys. **113**, 143509 (2013).
[20]J. B. DeLisio, F. Yi, D. A. LaVan, and M. R. Zachariah, J. Phys. Chem. C **121**, 2771 (2017).
[21]R. Armstrong, Combust. Sci. Technol. **71**, 155 (1990).
[22]R. Armstrong, Metall. Trans. A **23**, 2339 (1992).
[23]A. B. Mann, A. J. Gavens, M. E. Reiss, D. Van Heerden, G. Bao, and T. P. Weihs, J. Appl. Phys. **82**, 1178 (1997).
[24]A. J. Gavens, D. Van Heerden, A. B. Mann, M. E. Reiss, and T. P. Weihs, J. Appl. Phys. **87**, 1255 (2000).
[25]M. Salloum and O. M. Knio, Combust. Flame **157**, 288 (2010).
[26]M. Salloum and O. M. Knio, Combust. Flame **157**, 436 (2010).
[27]M. Salloum and O. M. Knio, Combust. Flame **157**, 1154 (2010).
[28]L. Alawieh, O. M. Kino, and T. P. Weihs, J. Appl. Phys. **110**, 013509 (2011).
[29]S. Jayaraman, O. M. Knio, A. B. Mann, and T. P. Weihs, J. Appl. Phys. **86**, 800 (1999).
[30]S. Jayaraman, A. B. Mann, M. Reiss, T. P. Weihs, and O. M. Knio, Combust. Flame **124**, 178 (2001).
[31]E. Besnoin, S. Cerutti, O. M. Knio, and T. P. Weihs, J. Appl. Phys. **92**, 5474 (2002).
[32]O. S. Rabinovich, P. S. Grinchuk, M. A. Andreev, and B. B. Khina, Physica B **392**, 272 (2007).
[33]I. E. Gunduz, K. Fadenberger, M. Kokonou, C. Rebholz, C. C. Doumanidis, and T. Ando, J. Appl. Phys. **105**, 074903 (2009).
[34]N. S. Weingarten, W. D. Mattson, A. D. Yau, T. P. Weihs, and B. M. Rice, J. Appl. Phys. **107**, 093517 (2010).
[35]F. Rizzi, M. Salloum, Y. M. Mazouk, R.-G. Xu, M. L. Falk, T. P. Weihs, G. Fritz, and O. M. Knio, Multiscale Model. Simul. **9**, 486 (2011).
[36]V. Turlo, O. Politano, and F. Baras, Acta Mater. **99**, 363 (2015).
[37]H.-Z. Wu and S.-J. Zhao, J. Alloys Compd. **581**, 519 (2013).
[38]M. L. Hobbs, D. P. Adams, and J. P. McDonald, WIT Trans. Eng. Sci. **61**, 127 (2008).
[39]F. R. de Boer, W. C. M. Mattens, R. Boom, A. R. Miedema, and A. K. Niessen, *Cohesion in Metals: Transition Metal Alloys* (North-Holland, Amsterdam, 1988).
[40]R. D. Murphy, R. V. Reeves, C. D. Yarrington, and D. P. Adams, Appl. Phys. Lett. **107**, 234103 (2015).

[41]W. M. Haynes, *CRC Handbook of Chemistry and Physics* (CRC Press, 2015), Vol. 96.
[42]J. R. Stewart and H. C. Edwards, in *Large-Scale PDE-Constrained Optimization* (Springer-Verlag, Berlin, 2003), pp. 301–315.
[43]A. P. Hardy and P. V. Phung, Combust. Flame **21**, 77 (1973).
[44]T. Boddington, F. Hongtu, P. G. Laye, M. Nawaz, and D. C. Nelson, Therochim. Acta **170**, 81 (1990).
[45]K. A. Philpot, Z. A. Munir, and J. B. Holt, J. Mater. Sci. **22**, 159 (1987).
[46]H. Kissinger, J. Res. Nat. Bur. Stand. **57**, 217 (1956).
[47]T. Akahira and T. Sunose, Research Report No. ■ (Chiba Institute of Technology, Evansville, 1971); Sci. Technol. **160**, ■ (1971).
[48]E. T. Swartz and R. O. Pohl, Appl. Phys. Lett. **51**, 2200 (1987).
[49]D. G. Naugle, J. Phys. Chem. Solids **45**, 367 (1983).
[50]Z. Radi, J. L. Labar, and P. B. Barma, Appl. Phys. Lett. **73**, 3220 (1998).

AQ2